EMI R&D PROJECT PROGRESS REPORT

All the following mandatory information needs to be provided. The length should *reflect the complexity and duration* of the project.

Reporting year	2026
Project Title:	**H**ydrogen **E**mission **S**cenarios to drive Climate **P**rojections for **E**nvironmental and **RI**sk **A**ssessment (**HESPERIA**)
Computer Project Account:	SPITBEAL
Principal Investigator(s):	Alessio Bellucci
Affiliation:	Consiglio Nazionale delle Ricerche, Istituto di Scienze dell'Atmosfera e del Clima (CNR-ISAC)
Name of ECMWF scientist(s) collaborating to the project (if applicable)	N/A
Start date of the project:	01/01/2025
Expected end date:	31/12/2027

Computer resources allocated/used for the current year and the previous one

(if applicable)

Please answer for all project resources

		Previous year		**Current year**	
		Allocated	Used	Allocated	Used
High Performance Computing Facility	(SBU)	2.8 Million	1.8 Million	10 Million	2.8 Million
Data storage capacity	(Gbytes)	4000	0	24000	952

Summary of project objectives (10 lines max)

HESPERIA aims to advance our understanding of the potential climate impacts of a hydrogen-based economy, using the state-of-the-art global climate model EC-Earth. The project specifically investigates how hydrogen emissions may influence Earth's radiative balance and evaluates the broader climate implications of hydrogen adoption across various socio-economic sectors. By exploring alternative scenarios with differing levels of hydrogen deployment, HESPERIA will generate new insights that complement existing scenario-based assessments from previous Coupled Model Intercomparison Project (CMIP) efforts—offering a timely and updated perspective on potential climate futures.

Summary of problems encountered (10 lines max)

There are no specific problems to be reported.

Summary of plans for the continuation of the project (10 lines max)

The upcoming semester (July-to-December 2026) will be dedicated to the following activities:

1. **Revise the implementation of stratospheric H2O perturbation** in IFS model, to address the lack of a distinctive radiative signature in the UH2O experiment.
2. Extend the set of AMIP experiments, using **alternative perturbation approaches**. The new experiments will consist in:
    - **Emission-driven perturbation approach**: apply to IFS the GHG (O3, CH4 and stratospheric H2O) perturbations associated to a 200 TgH2/year emission increase in the parent CTMs runs. This approach will result in a larger perturbation (hence, higher SNR) allowing the quantification of chemical non-linearities;
    - **Scaled concentration approach.** Scale the current double-H2-induced perturbations of GHG concentrations by a factor of 4-5, yielding a stronger radiative signal without chemical non-linearity.
3. Start the **implementation of climate change projections** using future GHG trajectories associated to a set of H2 emission scenarios, under low, medium and high levels of H2 deployment.

List of publications/reports from the project with complete references

……
……
……
……

Summary of results

Effective Radiative Forcing computation: experimental setup and CTM runs description

During this reporting period, the initially proposed experimental protocol to estimate the Effective Radiative Forcing (ERF) associated with the release of H2 in the atmosphere was further consolidated, and a first set of numerical simulations was performed. Specifically, we adopted a two-stage framework that combines offline chemistry–transport simulations with atmosphere-only integrations following the protocol designed for the Radiative Forcing Model Inter-comparison Project (RFMIP; Pincus et al., 2016). In this framework, composition changes diagnosed by chemistry models are prescribed to an atmospheric general circulation model run over fixed sea-surface boundary conditions, allowing the ERF to be diagnosed from the change in top-of-atmosphere (TOA) radiative fluxes after rapid atmospheric adjustments. The experimental design for ERF calculation is resumed below.

Stage 1: Chemistry–transport simulations

Tropospheric and stratospheric chemistry were simulated offline using the FRSGC/UCI and SLIMCAT Chemistry Transport Models (CTM), respectively. A reference simulation (BASELINE) was performed using hydrogen and methane concentrations representative of year 2010 (H_2 = 532 ppb and CH_4 = 1807 ppb, in global mean value).

Two perturbation experiments were then conducted. In the first (doubleH2), H_2 concentrations are doubled while CH_4 is held fixed at its baseline value, isolating the chemical impact of H_2 on ozone. In the second (doubleH2_fb), H_2 is doubled and CH_4 is increased to 1894 ppb to account for the methane feedback arising from OH perturbations. From these simulations we archived the three-dimensional changes in O_3, CH_4 and stratospheric H_2O, which represent the full chemically-mediated pathway by which H_2 influences radiation. A summary of the global mean H_2 and CH_4 concentration values adopted in the different CTM experiment is reported in Table 1. This set of simulations will be hereafter referred to as the *parent* simulations for the AMIP experiments, described in the following section.

Experiment ID	H2 conc (ppb)	CH4 level (ppb)
Baseline	532.6	1808
doubleH2	1065.3	1808
doubleH2_fb	1065.3	1894

Table 1. Summary table of H_2 and CH_4 concentration values adopted in the different CTM experiments.

Stage 2: AMIP ERF simulations

The chemical perturbations simulated by the CTMs were imposed in the ECMWF Integrated Forecasting System (IFS) operating in an AMIP configuration with repeating year-2010 sea-surface temperatures (SSTs) and sea-ice concentrations (SICs). Four 60-year simulations were conducted: a

control experiment (BASE) with unperturbed 2010 atmospheric composition; a simulation including O_3 perturbations only (DH2); a simulation including O_3 perturbations and the associated CH_4 feedback (DH2F); and a final simulation additionally incorporating the stratospheric H_2O response (UH2O). All other external forcings were held fixed at 2010 levels.

Effective radiative forcing was calculated from the difference in net TOA radiation between each perturbed simulation and BASE, thereby quantifying the radiative impact of hydrogen-induced changes in O_3, CH_4, and stratospheric H_2O.

Experiment ID	Parent CTM simulation	Perturbed O3	CH4 feedback	Perturbed H2O in stratosphere
BASE	Baseline	No	No	No
DH2	doubleH2	Yes	No	No
DH2F	doubleH2_fb	Yes	Yes	No
UH2O	doubleH2_fb	Yes	Yes	Yes

Table 2. List of AMIP experiments used to estimate ERF.

AMIP simulations with IFS model: ERF estimates

This section summarizes the results of the AMIP experiments listed in Table 2. We focus primarily on the DH2F and UH2O simulations, since the radiative response associated with the O_3-only perturbation (DH2) is small compared with the level of internal variability and cannot be robustly detected in the model simulations (not shown).

Figure 1 presents the evolution of the global-mean net TOA radiative flux as a function of averaging period. Values are expressed as anomalies relative to the corresponding BASE simulation, while uncertainty ranges are estimated using the standard error of the mean (SE=σ/N), where σ denotes the standard deviation and N the length of the record.

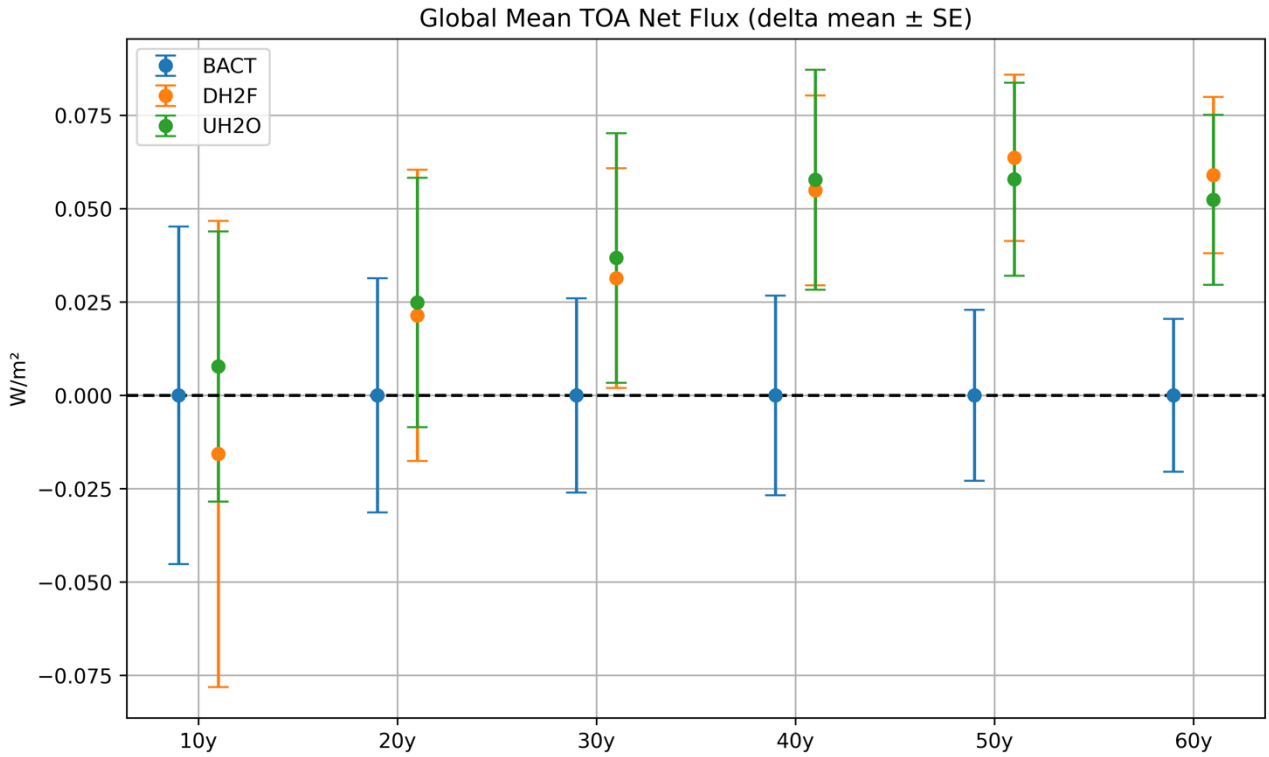

Fig. 1. Global-mean net TOA radiative flux (W/m^2) as a function of averaging period. Values are expressed as anomalies relative to the corresponding BASE simulation, while uncertainty ranges are estimated using the standard error of the mean (SE=σ/N), where σ denotes the standard deviation and N the length of the record.

Figure 1 highlights several important features of the ERF response. First, a statistically robust separation between the perturbed and control simulations emerges only after approximately 30–40 years of integration, reflecting the large level of internal variability in annual-mean TOA radiative fluxes. Beyond this timescale, the ERF estimate stabilizes, yielding a mean value of approximately +0.06 W m^{-2} for the doubled-H_2 perturbation. Normalizing by the corresponding H_2 burden increase (532 ppb; Table 1) gives an ERF efficiency of +0.11 mW m^{-2} ppb^{-1}, slightly lower than the value of +0.13 mW m^{-2} ppb^{-1} reported by Paulot et al. (2021).

A more unexpected result concerns the contribution of stratospheric water vapour. Differences between the DH2F and UH2O simulations are apparent during the first decade of integration but progressively diminish with increasing averaging period, leading to near-identical ERF estimates after several decades. This behavior suggests a negligible contribution of stratospheric H_2O to the diagnosed ERF, in contrast with current understanding of hydrogen-induced climate forcing. Previous studies (e.g. Paulot et al., 2021; Sand et al., 2023) indicate that stratospheric water vapour accounts for roughly 30% of the total ERF associated with H_2 perturbations. The apparent absence of such a contribution in the present simulations therefore warrants further investigation.

Next, we provide a closer view on the H2-induced radiative impact by looking at the spatial patterns of net TOA balance, comparing DH2F and UH2O against BASE experiments.

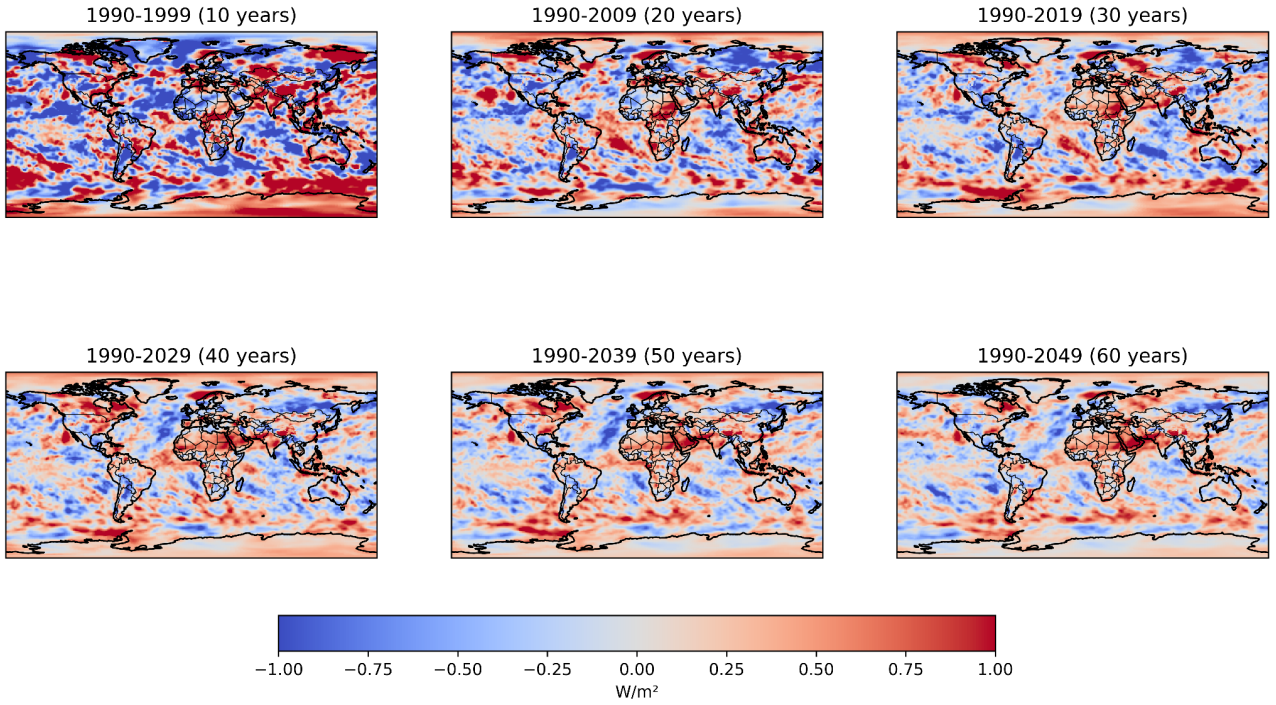

Figure 2. Net TOA radiative balance differences (W/m^2) between DH2F and BASE experiments calculated over increasing integration lengths (from 10 to 60 years).

Figure 2 shows the spatial distribution of net TOA radiative flux anomalies (DH2F minus BASE) calculated using averaging periods of increasing length. Positive (negative) values denote a net gain (loss) of energy by the climate system in the perturbed simulation relative to the control. As the averaging period increases from 10 to 60 years, the influence of internal variability is progressively reduced and coherent radiative forcing patterns begin to emerge.

The most prominent feature is the development of an extended region of positive TOA anomalies stretching across North Africa, the Arabian Peninsula, and the Indian subcontinent. This feature becomes clearly distinguishable only after approximately 40 years of integration, consistent with the timescale required for the global-mean ERF signal to emerge from background variability (Fig. 1). A second robust feature appears over the Southern Ocean as a zonally elongated band of positive anomalies, which also becomes increasingly evident with longer averaging periods.

The persistence and spatial coherence of these structures suggest that they reflect a genuine radiative response to the hydrogen-induced perturbations in atmospheric composition rather than sampling variability. Their emergence coincides with the stabilization of the global-mean ERF estimate, indicating that these regions contribute substantially to the positive TOA energy imbalance associated with enhanced atmospheric H_2.

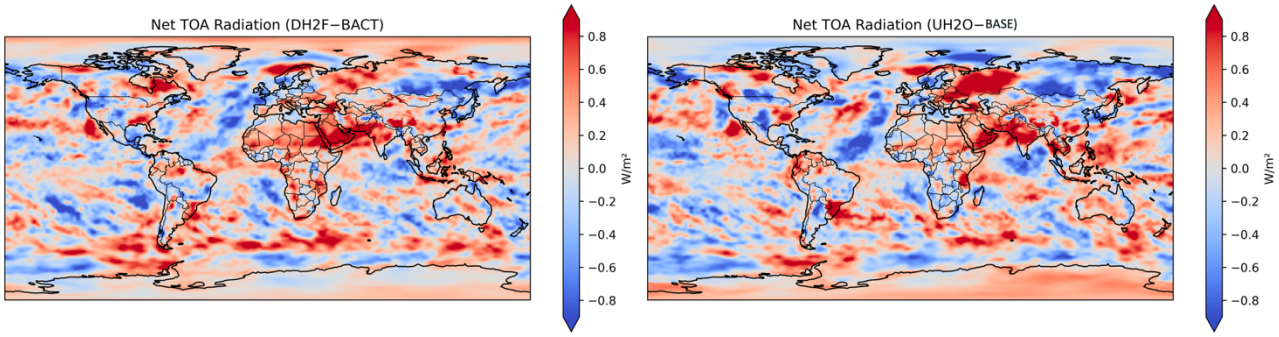

Figure 3. Net TOA radiative balance differences (W/m^2) between (left) DH2F and BASE, and (right) UH2O and BASE experiments calculated over the full integration length (60 years).

Next, we compare the two sensitivity experiments, with (UH2O) and without (DH2F) the contribution of H2O. Figure 3 shows the net TOA flux anomalies relative to BASE from UH2O (right) and DH2F (left), computed over the full 60-year integrations. As expected, the spatial pattern in UH2O shares several features with that in DH2F, but notable differences also emerge. For example, the pronounced positive radiative imbalance over eastern Africa, the Arabian Peninsula, and India, as well as the signal over the Southern Ocean, is evident in both simulations, suggesting a common origin associated with the radiative effects of O3 and CH4 perturbations. In contrast, UH2O exhibits a substantially enhanced radiative response over eastern Europe and Russia relative to DH2F, likely reflecting the additional contribution of stratospheric water vapor.

In summary, substantial progress was made during the reporting period towards quantifying the effective radiative forcing (ERF) associated with atmospheric hydrogen perturbations. Preliminary results are broadly consistent with previous studies, further supporting the conclusion that H_2 leakages can influence the Earth's radiative balance through indirect effects on the abundance of radiatively active species, including methane, ozone, and stratospheric water vapour. In the coming months, additional experiments will be performed to refine and strengthen the ERF assessment through alternative perturbation methodologies, while a new suite of simulations will investigate future climate responses under alternative hydrogen deployment pathways and associated emission scenarios.

References

Paulot, F. et al. Global modeling of hydrogen using GFDL-AM4.1: sensitivity of soil removal and radiative forcing. Int. J. Hydrog. Energy 46, 13446–13460 (2021).

Pincus, R., Forster, P. M., and Stevens, B.: The Radiative Forcing Model Intercomparison Project (RFMIP): experimental protocol for CMIP6, Geosci. Model Dev., 9, 3447–3460, https://doi.org/10.5194/gmd-9-3447-2016 (2016).

Sand, M., Skeie, R.B., Sandstad, M. et al. A multi-model assessment of the Global Warming Potential of hydrogen. Commun Earth Environ 4, 203 https://doi.org/10.1038/s43247-023-00857-8 (2023).